The PHB Granule Biogenesis Pathway in *Caulobacter*

Edward A. de Koning [a], Mayura Panjalingam [a], Jessica Tran [b], Michael R. Eckhart [b], Peter D. Dahlberg [c], Lucy Shapiro [a#]

[a]Department of Developmental Biology, Stanford University School of Medicine, Stanford, California, USA

[b]Stanford Protein and Nucleic Acid Facility, Stanford University School of Medicine, Stanford, California, USA

[c]Division of CryoEM and Bioimaging, SSRL, SLAC National Accelerator Laboratory, Menlo Park, California, USA.

Running Title: PHB Granule Biogenesis

#Correspondence: shapiro@stanford.edu

Abstract

PHB granules are bacterial organelles that store excess carbohydrates in the form of water-insoluble polyhydroxybutyrate (PHB). The PHB polymerase, phasin (a small amphipathic protein), and active PHB synthesis are essential for the formation of mature PHB granules in *Caulobacter crescentus*. Granule formation was found to be initiated by the condensation of self-associating PHB polymerase-GFP into foci, closely followed by the recruitment and condensation of phasin-mCherry. Following the active synthesis of PHB and granule maturation, the polymerase dissociates from mature granules and the PHB depolymerase is recruited to the granule. The polymerase directly binds phasin *in vitro* through its intrinsically disordered N-terminal domain. Thus, granule biogenesis is initiated and controlled by the action of a PHB polymerase and an associated helper protein, phasin, that together synthesize the hydrophobic granule content while forming the granule's protein boundary.

Importance

Like eukaryotes, bacteria organize their cytoplasm in subcellular compartments. These bacterial compartments can be membrane-bound (e.g. magnetosomes), or membraneless with protein-encased shells (e.g. carboxysomes). Here we investigate how *Caulobacter* forms membrane-less compartments that store the water-insoluble carbohydrate polymer polyhydroxybutyrate (PHB). A PHB polymerase is essential for granule biogenesis and we observed a direct interaction with the granule associated protein phasin through the disordered N-terminus of the polymerase. We found that PHB granules form by sequential recruitment of key proteins, beginning with the polymerase, and that the granule composition changes as these organelles mature.

Keywords: *Caulobacter*, bacterial organelle, PHB granule, PHB polymerase, phasin

41 **Introduction**

42

43 The compartmentalization of biochemical pathways in membrane bound subcellular organelles
44 is commonly observed in eukaryotic cells. Although membrane bound compartments are not
45 common in bacteria, there are instances of specific functions attributed to bacterial subcellular
46 compartments such as membrane bound magnetosomes (1) that sequester chemical
47 processes. Other bacterial subcellular organelles that are not membrane bound , include
48 protein encapsulated carboxysomes (2) and those that store polyhydroxy butyrate, PHB (3).
49 These granules are commonly found in many bacterial species, including *Caulobacter*
50 *crescentus* (4). Consumption of PHB is increased under carbon starvation, suggesting that
51 these granules function as carbohydrate storage organelles (5). Here, we have asked how a
52 new organelle is formed and identified the steps required for the *de novo* formation of
53 *Caulobacter* PHB granules.

54

55 Polymers of PHB are hydrophobic and highly insoluble in water. Due to its hydrophobicity,
56 accumulated PHB polymers could function as both the content of the organelle, and as its
57 selective boundary. However, Cryo-EM images have shown that this boundary is composed
58 of a discontinuous layer that is likely proteinaceous (6). Indeed, purified granules have been
59 found to consist mainly of PHB (>95%) and associated proteins (7, 8) and are generally
60 assumed to be membrane/lipid free (9). For an overview of PHB granule composition, see
61 Figure 1A.

62

63 The most abundant granule associated protein is phasin (PhaP), a 15-25 kDa helix-turn-helix
64 protein (10–12). Expression of phasin is regulated by the transcriptional repressor PhaR (13–
65 15). Helical wheel predictions of phasin suggest that the protein is amphipathic, which would
66 position the protein on the surface of the granule. It has been reported that phasin is localized
67 to granule surfaces and can encapsulate purified PHB *in vitro* (10, 16, 17). The crystal
68 structure of *Aeromonas hydrophila* phasin was recently solved revealing assemblies of phasins
69 in stacked hairpins such that the hydrophobic surfaces are shielded from the solution,
70 although it is not known if this conformation occurs *in vivo* on the surface of granules (18).
71 Another protein predicted to reside on the granule surface is the PHB polymerase (PhaC) that
72 catalyzes the polymerization of precursor monomers into PHB (19–21). The precursor
73 monomer is generated in two steps from acetyl-CoA by PhaA and PhaB to make (R)-3-
74 hydroxybutanoyl-CoA (3HB-CoA) (Fig 1A) (19, 22, 23).

75

76 PHB is in a crystalline state when synthesized *in vitro*, chemically extracted from PHB
77 containing bacteria, or found in the soil. In contrast, PHB in cells or in gently extracted
78 granules is amorphous (24–27). Bacterial PHB hydrolases can only degrade crystalline PHB
79 (28). Amorphous PHB is specifically degraded by a PHB depolymerase (PhaZ) (29), which is
80 found associated with mature PHB granules (30, 31). The mechanism that keeps PHB in an
81 amorphous state *in vivo* is unknown.
82
83 In this study we show that granule formation is dependent on the PHB polymerase (PhaC),
84 phasin (PhaP) and on the active accumulation of the PHB polymer. Granules are formed *de*
85 *novo* in *Caulobacter* by the initial condensation into foci of the PHB polymerase. The active
86 polymerase catalyzes the accumulation of PHB from the 3HB-CoA precursor. Further
87 accumulation of PHB is dependent on recruitment of phasin to the immature granule,
88 potentially by the direct interaction of polymerase and phasin, which we have shown occurs
89 *in vitro*. Granule biogenesis is stopped by departure of polymerase from the newly formed
90 granule, coincident with the recruitment of PhaZ depolymerase. Taken together, our
91 observations describe how the PHB granule is initiated and changes in composition during its
92 formation and maturation.
93
94 **Results**
95
96 *PHB granule formation requires both an active polymerase and phasin accumulation.*
97
98 PHB synthesis is dependent on the acetyl-CoA acetyltransferase PhaA (CCNA_00544) and
99 acetoacetyl-reductase PhaB (CCNA_00545) to produce the 3HB-CoA precursor from acetyl-
100 CoA (23). These genes have not been previously described in *Caulobacter* but are annotated
101 based on their homology. In *Caulobacter*, the polymerase PhaC (CCNA_01444) and the
102 depolymerase PhaZ (CCNA_00250) have been described previously (4, 32). For an overview
103 of PHB associated proteins, see Fig 1A. The only homologue to phasin found in *Caulobacter* is
104 CCNA_02242, or PhaP from here on. To validate these candidates, we made use of
105 hydrophobic dyes such as Nile Red and Nile Blue that have previously been reported to stain
106 for PHB in a wide variety of bacteria (33–35). We were able to stain PHB granules directly
107 with Nile Blue in the media, and with Nile Red after a PBS wash. We observed fluorescent
108 puncta in *Caulabacter* for both dyes, indicating the presence of PHB granules. These puncta
109 were absent in a mutant lacking the polymerase *phaC* gene and could be rescued by ectopic
110 expression of Polymerase-3xFLAG from a xylose inducible locus (Figs 1B and S1). In cells
111 where the transcription of *phaA* and *phaB* was controlled by a xylose inducible promotor, we

112 could tune the amount of available precursor. By reducing the amount of PhaA and PhaB
113 expression we observed a clear reduction in Nile Blue signal (Fig. 1C and 2A). This indicates
114 that not just the presence, but the activity of the PhaC polymerase is necessary for the Nile
115 Blue puncta. Deleting the phasin PhaP homologue in strain LS5812 also affects puncta
116 formation, as the number of puncta was reduced by 90% in this strain, which was rescued
117 upon ectopic expression of *phaP* from a xylose inducible locus (Figs. 1D and S1). Deletion of
118 the depolymerase did not affect the number of puncta per cell (Fig. 1B).
119
120 To further characterize the polymerase and phasin mutants, we imaged *Caulobacter* strains
121 using cryo-electron microscopy (cryo-EM). Analysis of Cryo-EM images of WT *Caulobacter*
122 cells show distributions of both small granules, consisting of poly-phosphate and PHB
123 granules, and large granules, which are exclusively PHB granules (Fig. S2 and Supplementary
124 Text). We observed that the deletion of *phasin* leads to a drastic reduction in larger PHB
125 granules, while simultaneously increasing the number of smaller (< 250nm diameter)
126 granules as compared to WT (Fig. S2). We cannot discern if the observed increase in smaller
127 granules in phasin deletion strains is due to an increase in poly-phosphate granules, or the
128 inability of smaller PHB granules to mature to larger PHB granules. We favor the latter
129 possibility; that we are observing a phasin-dependent maturation of smaller (<250nm
130 diameter) Nile Red negative, to larger (>250nm diameter) Nile Red positive PHB granules.
131
132 *Polymerase accumulation initiates granule biogenesis*
133
134 We used two separate approaches to study time dependent granule biogenesis. i) We
135 controlled the expression of precursor production by placing the phaA and *phaB* genes under
136 the control of the inducible xylose promoter (strain P_{xyl}-*phaAB*, Figs. 1C and 2A). In the
137 absence of xylose, granule biogenesis was prevented. While P_{xyl}-*phaAB* cells grown without
138 xylose do not have any Nile Blue stained granules, within 1 hour of xylose induction we clearly
139 observe Nile Blue stained granules (Fig. S3A). ii) Cells starved for glucose for at least 24hrs
140 results in a complete lack of Nile red stained granules (Fig. S3B), presumably due to the
141 consumption of all PHB. Reintroducing glucose in the medium restored Nile red-stained
142 granules within 3 hours (Fig. S3B). In each case, controlling precursor production or recovery
143 from starvation, provides a window of time to study *de novo* granule formation in *Caulobacter*.
144
145 Using timelapse microscopy, we followed polymerase-GFP and phasin-mCherry signal
146 condensation upon xylose induction of PhaAB expression in a strain containing both

147 fluorescent constructs (Fig. 2B). At the start of the experiment, coincident with the addition
148 of xylose, clear polymerase-GFP condensation is observed, while only faint phasin signal can
149 be detected. After 70 - 90 minutes of PhaAB induction, phasin-mCherry clearly co-localizes
150 with the polymerase. While the phasin-mCherry signal continues to accumulate as the granule
151 matures, the polymerase signal disappears after 2 hours of PhaAB induction.
152
153 The departure of the polymerase from a newly formed granule appears to coincide with the
154 mature granule's final size. We asked if this departure coincided with the recruitment of the
155 depolymerase, which is necessary for granule consumption. In cells recovering from
156 starvation, upon the addition of glucose at time 0, polymerase-GFP puncta were observed,
157 but no depolymerase-mCherry signal (Fig. 2C, t=0). The depolymerase-mCherry condenses
158 at the location of polymerase-GFP localization (Fig. 2B, t=135-180). The polymerase-GFP
159 signal continues to decrease at the first granule as depolymerase-mCherry signal increases,
160 and additional polymerase-GFP signal will condense to initiate the next granule formation (Fig.
161 2B, t=225-255). These results suggest that PHB granule composition changes over time,
162 initiated with polymerase condensation, followed by phasin accumulation and finally by the
163 recruitment of the depolymerase and loss of polymerase in older granules.
164
165 To ascertain that the polymerase condenses into loci prior to PHB accumulation, we used
166 cryo-CLEM (correlative light and electron microscopy) (36–38) with cells expressing GFP-
167 tagged PHB polymerase and stained with Nile Red to image PHB granules (Fig 3A). As shown
168 in Fig 3A, Nile Red exclusively stained larger granules with a diameter over 250nm, and Nile
169 Red intensity positively correlated with granule size (Fig. S4A). We observed that polymerase-
170 GFP localized to both smaller Nile Red negative and larger Nile Red positive granules (Fig. 3
171 and S4B) and was also observed independent of any granule. Thus, condensation of
172 polymerase precedes the accumulation of PHB polymer as detected by Nile Red. It should be
173 noted that some PHB is likely present in the smaller Nile Red negative granules, which could
174 be below the detection of Nile Red staining. Some membrane deformation can also be
175 observed in these Nile Red stained cells that are absent in unstained cells (see Fig. S2A),
176 possibly due to the PBS wash necessary for consistent Nile Red staining in our experiments.
177
178 The condensation of the polymerase to initiate nascent granule formation may be enhanced
179 by polymerase self-interaction. Using surface plasmon resonance, purified PHB polymerase
180 was tested for its ability to self-interact (Fig. 3B left panel). A strong response was observed

181 when increasing concentrations of polymerase are flown over surface-immobilized
182 polymerase, indicating a strong self-interaction of the PHB polymerase.
183
184 *The polymerase unstructured N-terminus binds phasin and is required for polymerase*
185 *expression*.
186
187 We have observed that polymerase condensation precedes the appearance of Nile Red-labeled
188 granules and that 3HB-CoA precursor production, and consequently polymerase catalyzed
189 PHB accumulation, is required for granule formation. We have also observed the continued
190 accumulation of phasin in maturing granules, and an inability of granules to mature in a *phasin*
191 deletion mutant (Fig. 2A and S2A). The inability of granules to increase in size in a *phasin*
192 mutant suggests a defect in maintaining PHB synthesis in the granule. This raises the possibly
193 that there is a promoting effect of phasin on polymerase activity, in turn increasing PHB
194 synthesis. To explain this putative self-reinforcing loop, we studied a potential interaction
195 between polymerase and phasin.
196
197 *Caulobacter* polymerase PhaC and phasin PhaP proteins were purified and used in surface
198 plasmon resonance experiments to determine if polymerase and phasin interacted *in vitro*.
199 (SPR, Fig. 4A). With phasin immobilized on the surface, we observed a polymerase
200 concentration-dependent response in signal (Fig. 4A, left graph). This concentration
201 dependent binding was also observed when the polymerase was immobilized on the surface
202 and the phasin flown over (Fig. S5). This direct interaction was surprising, since phasins in
203 two other bacterial species do not directly bind the polymerase when tested by BACTH or
204 crosslink pull-down (39, 40). However, the *Caulobacter* polymerase has an N-terminal,
205 intrinsically disordered domain that is not present in polymerase from either of the two
206 bacteria examined, *P. putida* or *C. necator* polymerase (41). Repeating the SPR with purified,
207 N-terminally truncated polymerase (polymeraseΔN, Table S1) revealed a complete lack of
208 binding with phasin (Fig. 4A, right graph). However, polymeraseΔN was still able to interact
209 with full-length polymerase (Fig. 3B, right graph).
210

211 **Discussion**

212

213 In this study, we asked how *Caulobacter* forms PHB granules *de novo*. The PHB polymerase
214 (PhaC) (4), the production of PHB monomers by PhaA and PhaB, and the phasin (PhaP)
215 homologue are essential for the formation and maturation of PHB granules in *Caulobacter*
216 (Fig. 1). Using timelapse fluorescent microscopy and correlative light and cryo-electron
217 microscopy (CLEM), we provide evidence that the composition of PHB granules changes over
218 time as the granule matures (Figs. 2,3). We further used surface plasmon resonance to show
219 that purified PHB polymerase and phasin interact directly through an N-terminal extension of
220 the PHB polymerase that is unique to *Caulobacter.* Based on our results, we propose a model
221 of PHB granule biogenesis and maturation in *Caulobacter* (Fig. 4B): i) Polymerase self-
222 interaction (Fig. 3B) promotes condensation that precedes the condensation of phasin (Fig.
223 2B). ii) The polymerase can recruit phasin through its N-terminus (Fig. 4A) and form a nascent
224 granule, possibly assisted by the early initiation of PHB polymer formation. iii) Ongoing PHB
225 synthesis expands the granule size and the granule surface. iv) As the granule grows to its
226 mature size, more phasin is recruited to the granule (Fig. 2B). v) Once the granule reaches
227 its mature size, the PHB polymerase dissociates from the granule, coinciding with the
228 recruitment of the PHB depolymerase (Fig 2C).

229

230 The sequential localization of granule associated proteins illustrates that the composition of
231 individual PHB granules changes over time, similar to changes in the composition of
232 magnetosomes and carboxysomes during their formation (1, 2, 42). Magnetosomes are
233 membrane bound organelles in which magnetite is stored, enabling their magnetotactic
234 bacterial hosts to orient themselves within a magnetic field, assisting in chemotaxis (1, 43,
235 44). During magnetosome biogenesis, the bacterial inner membrane invaginates to form a
236 compartment, followed by the accumulation of magnetite (1, 45, 46). Carboxysomes, which
237 carry out carbon fixation and are responsible for efficient photosynthesis under low CO_2
238 concentrations, are not encapsulated by a membrane. The key photosynthetic protein,
239 RuBisCo, is first condensed into a pre-carboxysome. Shell proteins are then recruited to
240 encapsulate this condensate generating a finished carboxysome (2, 47). PHB granules are not
241 membrane bound, but there is also no evidence of a continuous protein shell (6, 9). As active
242 PHB synthesis is required for granule formation, PHB 'seeds' emerging from the polymerase
243 condensation, possibly aided by condensation of the disordered N terminal portion of the
244 polymerase prior to granule formation, could help drive initial accumulation. Considering PHB
245 is highly water insoluble, phase transition could function as a selective barrier for this

organelle. This interface between cytoplasm and PHB is the most likely site for accumulation of granule associated proteins. Since PHB synthesis is required for granule formation, the volume to surface ratio changes as a granule increases in size. This ratio could play a role in selective protein recruitment to the granule surface.

The recruitment of depolymerase (PhaZ) following that of the polymerase answers a previous paradox of futile PHB cycling (48, 49). Published studies observed the expression of both PHB polymerase and depolymerase in cell cultures, suggesting that PHB is both formed and consumed (50, 51). Purified granule populations also show the presence of both polymerase and depolymerase (8). However, in both cases an ensemble measurement was made. In our single cell imaging experiments, we observed that while PHB polymerase and depolymerase can be expressed in the same cell, they do not necessarily co-localize to the same granule at the same time in granule maturation. (Fig 2).

Phasin isolated from *Pseudomonas putida* has been shown to encapsulate PHB *in vitro* (17), and, *in vivo*, phasin protein levels were found to increase during PHB production in *C. necator* and *Caulobacter* (13, 52). *In vitro* reactions of PHB synthesis occur in large (about a centimeter) aggregates indicating the tendency of PHB to self-associate (53). Further, a previous cryo-EM study suggested that the bimodal distribution of granules size might indicate granule fusion *in vivo* (6). Thus, it is possible that PHB granules fuse and that this fusing is coordinated by phasin, although granule fusion has so far not been observed directly. Deletion of *Caulobacter* phasin disrupts the formation of mature granules, and instead leads to the accumulation of what may be small immature granules (Fig. S2). Because of the observed sequential recruitment of polymerase and phasin (Fig 2), the smaller size of PHB granules in a *phasin* mutant could indicate a premature departure of polymerase from this granule. Thus, changes in the number and size of granules likely reflect differences in the rate of granule initiation, granule growth, and departure of polymerase from existing granules. The role of phasin could be to control both the activity and retention of the polymerase at the granule, thereby influencing the final size of mature granules. The direct interaction between phasin and polymerase likely contributes to the retention of polymerase on the granule, in addition to the initial recruitment of phasin by polymerase.

Strong polymerase self-interaction, measured by SPR (Fig 3B), likely contributes to its localized accumulation and the initiation of granule formation. Since PHB synthesis is required for granule formation (Fig 1), cells can control granule formation by directly controlling

281 polymerase activity. Phosphorylation of the polymerase has been reported to control PHB
282 synthesis in *C. necator* (54). However, the reported phosphorylated threonine residue (T373)
283 is not conserved in *Caulobacter.* An alternative method of polymerase regulation could be
284 through degradation. We had limited success detecting a truncated polymeraseΔN version in
285 *Caulobacter* with either Western blot (FLAG-tagged) or fluorescent microscopy (GFP-tagged)
286 (data no shown). However, there was no difficulty purifying these proteins when expressed
287 in *E. coli*. This could indicate the presence of a *Caulobacter* specific degradation pathway to
288 control the polymerase activity, and by extension PHB granule biogenesis.
289
290 The polymerase N-terminus directly binds phasin, which may play a role in phasin's
291 recruitment to the PHB granule, and in retention of the polymerase at the PHB granule by
292 phasin. The intrinsically disordered N-terminal extension of the polymerase is unique to
293 *Caulobacter*, but the N-terminal region shows sequence and functional homology to PhaM in
294 *C. necator*. PhaM contains an intrinsically disordered region comprised of lysine, proline, and
295 alanine repeats (55), which is also found in the *Caulobacter* polymerase N-terminus. It has
296 been reported that *Caulobacter* polymeraseΔN protein lacking this disordered region shows a
297 lag in *in vitro* PHB synthesis (41), like that observed for *C. necator* polymerase (41). Addition
298 of PhaM to the *C. necator* polymerase was reported to overcome this initial lag phase (56),
299 analogous to the absence of lag phase reported for the full length *Caulobacter* polymerase
300 (41). PhaM has been shown to associate with PHB granules, and in mutants lacking PhaM
301 fewer PHB granules are observed (3, 57). Thus, the intrinsically disordered N-terminus of the
302 *Caulobacter* polymerase functions in a manner analogous to the disordered *C. necator* PhaM
303 protein. This underscores a possible role for the N-terminal region of the *Caulobacter*
304 polymerase in the initiation of granule biogenesis. The intrinsically disordered region and
305 polymerase self-interaction may enable localized phase transition which then facilitates the
306 recruitment of the phasin necessary for granule maturation.
307
308 PHB granule formation appears to be highly regulated and intricately linked to central carbon
309 metabolism in *Caulobacter*. Precursor synthesis from acetyl-CoA directly links granule
310 formation and growth to the metabolic state of the cell, possibly functioning as an overflow
311 metabolite. If there is no need to make PHB, no organelle will be formed. Phasin is essential
312 for the continued maturation of the PHB granule, potentially by promoting polymerase activity
313 or polymerase retention at the granule. Phasin expression is regulated by the repressor PhaR
314 (13, 58), and PhaR has been reported to bind both DNA and PHB (59). Sequestration of PhaR
315 to the PHB granule has been previously proposed as a mechanism to relieve repression of

316 *phasin* transcription (15), ensuring that phasin is only produced under conditions that promote
317 PHB synthesis. Thus, transcriptional regulation of *phasin* by PhaR ensures proper timing of
318 phasin expression to occur only at the time of granule maturation. In the absence of this
319 additional phasin, the granule is unable to mature, possibly due to premature departure of
320 the polymerase from the granule boundary. As part of the granule boundary, this puts the
321 PHB polymerase at the center of organelle formation; ensuring that its enzymatic activity
322 continues at the granule surface where it directly dictates PHB granule formation and growth,
323 while departure of the polymerase determines the final size of the mature granule.
324

Material and Methods

Bacterial growth conditions

Unless stated otherwise *Caulobacter* strains were inoculated from glycerol stock in PYE for overnight growth at 30°C under aeration. Antibiotics were used for selection during strain construction and added for selective pressure for single-crossover integrated constructs. Antibiotic concentrations that were used (liquid/solid): spectinomycin (25/50 µg/ml), kanamycin (5/25 µg/ml), rifampicin (2.5/5 µg/ml), gentamicin (0.5/5 µg/ml), tetracycline (1/1 µg/ml) and chloramphenicol (2/1 µg/ml). *Escherichia coli* strains were inoculated from glycerol stock in LB for overnight growth at 37°C under aeration. The following concentrations of antibiotics were used for *E. coli*: spectinomycin (50/100 µg/ml), kanamycin (50/50 µg/ml), rifampicin (25/50 µg/ml), gentamicin (15/20 µg/ml), tetracycline (12/12 µg/ml) and chloramphenicol (20/30 µg/ml). All strains used in this study are listed in table S1.

Plasmid and strain construction

Plasmids were constructed using previously reported plasmids (60). Plasmids used in this study were either; i) ordered from Synbio Technologies, ii) constructed using Gibson Assembly (GA) protocol from New England Biolabs (NEB) or iii) using restriction-ligation per NEB protocol. Plasmids and primers used in this study are listed in table S2. Plasmids were isolated using Monarch Plasmid Miniprep kit from NEB and linearized using restriction enzyme by NEB as per manufacturer's protocol. Inserts were acquired by PCR using KOD Hotstart Mastermix from NovaGen and purified from gel using Monarch DNA Gel Extraction kit from NEB. All cloning was performed in *E. coli* using ultracompetent DH5α from NEB by heat shock as per manufacturer's protocol. Plasmids were transformed to *Caulobacter* by electroporation. For marker-free integration and deletion, plasmids were first integrated selecting for kanamycin resistance, after which counter-selection on sucrose was performed (60). Kanamycin sensitive candidates were verified by PCR.

pEK001 was constructed by 2 fragment GA using pET28a linearized with BamHI and NheI as backbone and CCNA_01444 amplified from gDNA with EKP001 and EKP002 as insert. pEK003 was constructed by 4 fragment GA using pNTPS138 linearized by HindIII and NheI, *CCNA_02242* CDS without stop codon including 368bp upstream amplified from gDNA genomic DNA (gDNA) with EKP005 and EKP006, mCherry amplified from pCHYC-1 with EKP007 and EKP008, and 800bp downstream of *CCNA_02242* amplified from gDNA with EKP009 and EKP010. pEK005 was constructed by Synbio using PCR cloning, combining synthesized *CCNA_01444* 3' 800bp into pGFPC-4 backbone. pEK011 was constructed by Synbio using gene synthesis using pET28a as a backbone and *CCNA_02242* as synthesized

360 insert. pEK012 was constructed by Synbio using gene synthesis, combining the fragments
361 800bp upstream *CCNA_02242*, the chloramphenicol cassette from pMCS-6, and 800bp
362 downstream of *CCNA_02242* into pNPTS138. pEK013 was constructed by Synbio using gene
363 synthesis, combining 800bp upstream of *CCNA_00250*, the tetracycline cassette from pMCS-
364 5, and 800bp downstream of *CCNA_00250* into pNPTS138. pEK014 was constructed by Synbio
365 using gene synthesis, combing 800bp upstream of *CCNA_01444*, the rifampicin cassette from
366 pMCS-3, and 800bp downstream of *CCNA_01444* into pNPTS138. pEK022 was constructed by
367 2 fragment GA using backbone pXMCS-2 linearized with KpnI and NdeI and insert 5' 800bp
368 of *CCNA_00544* amplified with EKP015 and EKP016 from gDNA. pEK035 was constructed by
369 amplifying pEK001 using EKP040 and EKP041, digesting the PCR product with NheI and
370 ligating the ends back together. pEK044 was constructed by 4 fragment GA, using pNPTS138
371 linearized with HindIII and NheI as backbone, 3' 800bp of CCNA_00250 amplified with MP001F
372 and MP002R from gDNA, mCherry amplified from pCHYC-1 with MP002F and MP002R, and
373 800bp downstream of CCNA_00250 amplified with MP003F and MP003R from gDNA. pEK052
374 was constructed by 2 fragment GA, using pTC127 linearized by NdeI and SacI as a backbone,
375 and CCNA_01444 amplified from gDNA with EKP083 and EKP084 as insert. pEK055 was
376 constructed by 2 fragment GA, using pXCHYC-2 linearized with NdeI and NheI as backbone,
377 and CCNA_02242 amplified from gDNA with EKP071 and EKP074 as insert.
378
379 *Staining of PHB granules*
380 *Caulobacter* cells were inoculated from glycerol stock into PYE and grown overnight at 30°C.
381 Overnight cultures were subcultured in M2G minimal media and grown overnight at 30°C. For
382 nile red staining, cells were washed in PBS and stained in PBS and 1μM Nile Red (final
383 concentration) for 20 minutes at room temperature. Cells were washed in PBS and
384 subsequently imaged. For Nile Blue staining, 10μM Nile Blue (final concentration) was added
385 directly to the media and cells were stained for 20 minutes at room temperature. Cells were
386 washed in M2G and subsequently imaged.
387
388 *Room-temperature fluorescent microscopy and image analysis*
389 Unless otherwise stated, cells were imaged on M2G 1% agarose pads on a Leica Dmi8
390 multicolor epifluorescence microscope. A phase-contrast 100x oil immersion objective was
391 used with a Lumencor SpectraX LED light source. Images were captured on an EMCCD camera
392 (Hamamatsu C9100 02 CL). GFP was imaged at 480nm excitation and 527nm emission.
393 mCherry, nile red and PHB specific nile blue were imaged at 554nm excitation and 609nm

394 emission. Nile blue membrane stain was imaged at 635nm excitation and 680nm emission.
395 Images were analyzed and quantified using ImageJ (Fiji).
396
397 *Cryogenic electron microscopy*
398 Single cryogenic transmission electron micrographs of *C. crescentus* were acquired using a
399 300 keV electron microscope (G3 Titan Krios™) equipped with direct electron detection
400 camera with a BioQuantum™ Imaging Filter (Gatan, Inc) using a 30-eV slit width. The
401 effective pixel size was ~6.5 Å, target defocus was 10 µm and the total dose was 25 $e^-/Å^2$.
402 For presentation the data was binned by 4 into 2.6 nm pixels. Acquisitions were controlled
403 using SerialEM software (61).
404
405 *Cryogenic correlative light and electron tomography*
406 Cryogenic light microscopy for correlative imaging was acquired on a home-built light
407 microscope (62). Light microscopy was performed using either 488 nm (imaging of GFP
408 channel) or 561 nm (imaging of nile red channel) laser-based illumination through a 100x
409 objective (Nikon CFI TU Plan Apo 100x/NA0.9). Intensities at the sample were kept below 50
410 W/cm^2 to avoid sample heating and devitrification(63). Fluorescent emission was detected
411 with an EMCCD camera (Andor iXon) after passing through a 488 nm and 561 nm notch
412 blocking filters and either a 525/50 bandpass for the GFP channel or 607/70 bandpass filter
413 for the nile red channel. Despite both color channels being collected on the same detector,
414 slight shifts in the relative position of the images were corrected for by translating one color
415 channel to align common features, such as grid holes, for each field of view. The excitation
416 beam profiles were measured using a thin film of fluorescent dye embedded in PVA-VA spun
417 on a coverslip. Fluorescent brightness across the field of view was corrected for by dividing
418 acquired images by a Gaussian fit to the measured beam profiles.
419 Subsequent electron tomography was performed on a 300 keV electron microscope (G3 Titan
420 Krios™) equipped with direct electron detection camera with a BioQuantum™ Imaging Filter
421 (Gatan, Inc) using a 20-eV slit width. The effective pixel size was 4.49 Ångstroms. The tilt
422 series was acquired unidirectionally over ±46 degrees in 2 degree steps. Total dose was 100
423 $e^-/Å^2$. Reconstructions were performed using IMOD with data binned-by-4 to produce 1.8 nm
424 effective pixels (64). Registration of light microscopy and electron tomography datasets was
425 performed using a projective transformation first to a lower magnification cryoEM micrograph
426 and then a similar transformation to the higher magnification tomography datasets. Further
427 details on the registration process can be found in Dahlberg et al (38).
428

429 *Timelapse microscopy*

430 Overnight PYE cultures of *Caulobacter* were subcultured in M2G minimal media and grown at
431 30°C overnight. For xylose induction, the cells were pelleted and resuspended in M2G+0.1%
432 xylose and spotted on M2G+0.1% xylose pads. For glucose recovery, the culture was washed
433 in M2 and resuspended in M2 and starved 24 hours at 30°C. Just prior to imaging, cells were
434 pelleted and resuspended in M2G and spotted on M2G pads. The coverslip was sealed by wax
435 to prevent evaporation and the recovering cells were imaged at 10-minute (xylose induction)
436 or 15-minute (starvation recovery) intervals for at least 3 hours.

437

438 *Protein purification*

439 His-tagged proteins were expressed in *E. coli* BL21(DE3) using the pET28a system
440 (polymerase = pEK001, phasin = pEK011 and polymeraseΔN = pEK035). Cells were grown
441 overnight at 37°C in LB and diluted 1:400 into prewarmed LB. At an OD_{600} of approximately
442 0.5, protein expression was induced with 0.4μM IPTG and the culture was shifted to 18°C for
443 another 3 hours. Cells were washed in ice-cold PBS and the pellet was stored at -80°C. Cells
444 were thawed on ice and resuspended in ice-cold lysis buffer (50mM HEPES-KOH pH 8.0,
445 500mM KCl, 25mM imidazole, 1 protease tablet per 50mL buffer, 200U benzonase nuclease
446 at 0.3ul per 1L culture). Cells were lysed by sonication (3 sec pulse, 12 sec rest, 100%
447 amplitude, 4 minute total pulse) and the lysate was cleared by centrifugation (30 minutes,
448 4°C at 29000 rcf). Cleared lysate was inoculated with pre-equilibrated Ni-NTA resin (1ml per
449 1l culture) for 2 hours at 4°C under gentle agitation. The lysate-resin mixture was separated
450 by a gravity column (Poly-Prep Chromatography Column, Bio-Rad) and the resin was washed
451 with 15 column volumes (CV) wash buffer (50mM HEPES-KOH pH 8.0, 500mM KCl, 25mM
452 imidazole). The sample was eluted in 5 CV elution buffer (50mM HEPES-KOH pH 8.0, 500mM
453 KCl, 250mM imidazole, 10% glycerol) and stored at -80°C. For the removal of the His6-tag,
454 a Thrombin CleanCleave Kit (Sigma) was used.

455

456 *Surface Plasmon Resonance*

457 Reagents: Sensor CM5 chips, N-Hydroxysuccinimide (NHS), 1-Ethyl-3-(3-
458 dimethylaminopropyl) carbodiimide (EDC), and ethanolamine hydrochloride (EA) were
459 obtained from GE Healthcare/Cytiva. Surface Plasmon Resonance experiments were
460 performed on a BIACORE 3000 biosensor system (GE Healthcare/Cytiva) at 25ºC. Proteins
461 were dialyzed against Assay Buffer (20mM HEPES pH7.4, 200mM NaCl) before use. The
462 different proteins (His-tagged or untagged Polymerase (PhaC) and phasin (PhaP)) were
463 covalently immobilized on the surface of a CM5 biosensor chip (GE Healthcare/Cytiva) by

amine coupling chemistry using N-hydroxysuccinimide (NHS) and N'-(3-dimethylaminopropyl) carbodiimide hydrochloride (EDC) according to the manufacturer's instructions. To investigate binding of Polymerase (PhaC) or phasin (PhaP) to the immobilized Polymerase (PhaC) or phasin (PhaP), dialyzed proteins were diluted in Assay Buffer and injected over the Ligand containing surface for 2min at different concentrations at a flow rate of 30 µl/min. For each experiment at least 5 different concentrations of analyte proteins were injected over each experimental and control flow cell. Dissociation was allowed to occur at the same flow rate for 300 sec. followed by Regeneration Buffer (20mM HEPES pH7.4, 1M NaCl) at a flow rate of 100 µl/min for 30sec and Assay Buffer alone at a flow rate of 30 µl/min to allow the baseline to stabilize. All data were corrected for unspecific binding by subtracting the signal measured in a control cell lacking immobilized ligand. Data analysis was performed using the BIAevaluation software 4.1 (GE Healthcare/Cytiva).

Acknowledgements: We thank T. Chong for providing plasmids and thank T. Chong and S. Saurabh for helpful discussions on experimental aspects of the manuscript. We thank all members of the Shapiro laboratory for constructive feedback throughout this work. **Funding:** This work was supported by the National Institutes of Health (R35-GM118071 to L.S). L.S. is a Chan Zuckerberg Biohub Investigator. P.D.D. was supported in part by the Panofsky Fellowship at the SLAC National Accelerator Laboratory as part of the Department of Energy Laboratory Directed Research and Development program under contract DE-AC02-76SF00515 and by grant 2021-234593 from the Chan Zuckerberg Initiative DAF, an advised fund of Silicon Valley Community Foundation. **Author contributions:** This study was conceived by E.A.K. Experiments were designed by E.A.K., with input from L.S., M.E. and P.D.D. Strains for this study were engineered by E.A.K. and M.P. Room temperature fluorescent microscopy was performed by E.A.K. and M.P and analyzed by E.A.K. Protein purification and BACTH were done by E.A.K. SPR was performed by J.T. and M.R.E. and analyzed by M.R.E. and E.A.K. Cryo-EM and CLEM measurements were performed and analyzed by P.D.D. and E.A.K. The manuscript was written by E.A.K. and L.S., with input from P.D.D. and M.R.E. **Competing interests:** The authors declare that they have no competing interests. **Data and material availability:** Plasmids and strains used and created for this work can be obtained on request.

References

1. Komeili A, Li Z, Newman DK, Jensen GJ. 2006. Magnetosomes Are Cell Membrane Invaginations Organized by the Actin-Like Protein MamK. Science (80-) 311:242–

499 246.
500 2. Cameron JC, Wilson SC, Bernstein SL, Kerfeld CA. 2013. Biogenesis of a bacterial
501 organelle: The carboxysome assembly pathway. Cell 155:1131.
502 3. Jendrossek D, Pfeiffer D. 2014. New insights in the formation of
503 polyhydroxyalkanoate granules (carbonosomes) and novel functions of poly(3-
504 hydroxybutyrate). Environ Microbiol 16:2357–2373.
505 4. Qi Q, Rehm BHA. 2001. Polyhydroxybutyrate biosynthesis in Caulobacter crescentus:
506 molecular characterization of the polyhydroxybutyrate synthase. Microbiology
507 147:3353–3358.
508 5. Anderson AJ, Dawes EA. 1990. Occurrence, metabolism, metabolic role, and industrial
509 uses of bacterial polyhydroxyalkanoates. Microbiol Rev 54:450–472.
510 6. Beeby M, Cho M, Stubbe J, Jensen GJ. 2012. Growth and localization of
511 polyhydroxybutyrate granules in ralstonia eutropha. J Bacteriol 194:1092–1099.
512 7. Griebel R, Smith Z, Merrick JM. 1968. Metabolism of Poly-β-hydroxybutyrate. I.
513 Purification, Composition, and Properties of Native Poly-β-hydroxybutyrate Granules
514 from Bacillus megaterium. Biochemistry 7:3676–3681.
515 8. Sznajder A, Pfeiffer D, Jendrossek D. 2015. Comparative proteome analysis reveals
516 four novel polyhydroxybutyrate (PHB) granule-associated proteins in Ralstonia
517 eutropha H16. Appl Environ Microbiol 81:1847–1858.
518 9. Bresan S, Sznajder A, Hauf W, Forchhammer K, Pfeiffer D, Jendrossek D. 2016.
519 Polyhydroxyalkanoate (PHA) granules have no phospholipids. Sci Rep 6:1–13.
520 10. Pieper-Furst U, Madkour MH, Mayer F, Steinbuchel A. 1995. Identification of the
521 region of a 14-kilodalton protein of Rhodococcus ruber that is responsible for the
522 binding of this phasin to polyhydroxyalkanoic acid granules. J Bacteriol 177:2513–
523 2523.
524 11. Wieczorek R, Steinbüchel A, Schmidt B. 1996. Occurrence of polyhydroxyalkanoic acid
525 granule-associated proteins related to the Alcaligenes eutrophus H16 GA24 protein in
526 other bacteria. FEMS Microbiol Lett 135:23–30.
527 12. Wieczorek R, Pries A, Steinbuchel A, Mayer F. 1995. Analysis of a 24-kilodalton
528 protein associated with the polyhydroxyalkanoic acid granules in Alcaligenes
529 eutrophus. J Bacteriol 177:2425–2435.
530 13. York GM, Stubbe J, Sinskeyl AJ. 2002. The ralstonia eutropha PhaR protein couples
531 synthesis of the PhaP phasin to the presence of polyhydroxybutyrate in cells and
532 promotes polyhydroxybutyrate production. J Bacteriol 184:59–66.
533 14. Chou ME, Yang MK. 2010. Analyses of binding sequences of the PhaR protein of

534 Rhodobacter sphaeroides FJ1. FEMS Microbiol Lett 302:138–143.
535 15. Jendrossek D. 2009. Polyhydroxyalkanoate granules are complex subcellular
536 organelles (carbonosomes). J Bacteriol 191:3195–3202.
537 16. Neumann L, Spinozzi F, Sinibaldi R, Rustichelli F, Pötter M, Steinbüchel A. 2008.
538 Binding of the major phasin, PhaP1, from Ralstonia eutropha H16 to poly(3-
539 hydroxybutyrate) granules. J Bacteriol 190:2911–2919.
540 17. Mato A, Tarazona NA, Hidalgo A, Cruz A, Jiménez M, Pérez-Gil J, Prieto MA. 2019.
541 Interfacial Activity of Phasin PhaF from Pseudomonas putida KT2440 at Hydrophobic-
542 Hydrophilic Biointerfaces. Langmuir 35:678–686.
543 18. Zhao H, Wei H, Liu X, Yao Z, Xu M, Wei D, Wang J, Wang X, Chen GQ. 2016.
544 Structural Insights on PHA Binding Protein PhaP from Aeromonas hydrophila. Sci Rep
545 6:1–13.
546 19. Liebergesell M, Sonomoto K, Madkour M, Mayer F, Steinbüchel A. 1994. Purification
547 and Characterization of the Poly(Hydroxyalkanoic Acid) Synthase from Chromatium
548 vinosum and Localization of the Enzyme at the Surface of Poly(Hydroxyalkanoic Acid)
549 Granules. Eur J Biochem 226:71–80.
550 20. Wittenborn EC, Jost M, Wei Y, Stubbe JA, Drennan CL. 2016. Structure of the catalytic
551 domain of the class I polyhydroxybutyrate synthase from Cupriavidus necator. J Biol
552 Chem 291:25264–25277.
553 21. Arsad H, Chek MF, Samian MR, Hakoshima T, Sudesh K, Mori T, Kim S-Y. 2017.
554 Structure of polyhydroxyalkanoate (PHA) synthase PhaC from Chromobacterium sp.
555 USM2, producing biodegradable plastics. Sci Rep 7:1–15.
556 22. Gerngross TU, Martin DP. 1995. Enzyme-catalyzed synthesis of poly[(R)-(-)-3-
557 hydroxybutyrate]: formation of macroscopic granules in vitro. Proc Natl Acad Sci
558 92:6279–6283.
559 23. Slater SC, Voige WH, Dennis DE. 1988. Cloning and expression in Escherichia coli of
560 the Alcaligenes eutrophus H16 poly-β-hydroxybutyrate biosynthetic pathway. J
561 Bacteriol 170:4431–4436.
562 24. Merrick JM, Doudoroff M. 1964. DEPOLYMERIZATION OF POLY-beta-
563 HYDROXYBUTYRATE BY AN. J Bacteriol 88:60–71.
564 25. Lauzier C, Marchessault RH, Smith P, Chanzy H. 1992. Structural study of isolated
565 poly(β-hydroxybutyrate) granules. Polymer (Guildf) 33:823–827.
566 26. Kawaguchi Y, Doi Y. 1990. Structure of native poly(3-hydroxybutyrate) granules
567 characterized by X-ray diffraction. FEMS Microbiol Lett 70:151–155.
568 27. Horowitz DM, Sanders JKM. 1994. Amorphous, Biomimetic Granules of

569 Polyhydroxybutyrate: Preparation, Characterization, and Biological Implications. J Am
570 Chem Soc 116:2695–2702.
571 28. Gebauer B, Jendrossek D. 2006. Assay of poly(3-hydroxybutyrate) depolymerase
572 activity and product determination. Appl Environ Microbiol 72:6094–6100.
573 29. Jendrossek D, Knoke I, Habibian RB, Steinbüchel A, Schlegel HG. 1993. Degradation
574 of poly(3-hydroxybutyrate), PHB, by bacteria and purification of a novel PHB
575 depolymerase from Comamonas sp. J Environ Polym Degrad 1:53–63.
576 30. Saegusa H, Shiraki M, Kanai C, Saito T. 2001. Cloning of an intracellular Poly[D(-)-3-
577 hydroxybutyrate] depolymerase gene from Ralstonia eutropha H16 and
578 characterization of the gene product. J Bacteriol 183:94–100.
579 31. de Eugenio LI, García P, Luengo JM, Sanz JM, Román JS, García JL, Prieto MA. 2007.
580 Biochemical evidence that phaZ gene encodes a specific intracellular medium chain
581 length polyhydroxyalkanoate depolymerase in Pseudomonas putida KT2442. J Biol
582 Chem 282:4951–4962.
583 32. Dufresne ER, Cabeen MT, Jacobs-Wagner C, Parry BR, Surovtsev IV, O'Hern CS.
584 2013. The Bacterial Cytoplasm Has Glass-like Properties and Is Fluidized by Metabolic
585 Activity. Cell 156:183–194.
586 33. Ostle AG, Holt JG. 1982. Fluorescent Stain for Poly-3- Hydroxybutyrate. Appl Environ
587 Microbiol 44:238–241.
588 34. Spiekermann P, Rehm BHA, Kalscheuer R, Baumeister D, Steinbüchel A. 1999. A
589 sensitive, viable-colony staining method using Nile red for direct screening of bacteria
590 that accumulate polyhydroxialkanoic acids and other lipit storage compounds. Arch
591 Microbiol 171:73–80.
592 35. Juengert J, Bresan S, Jendrossek D. 2018. Determination of Polyhydroxybutyrate
593 (PHB) Content in Ralstonia eutropha Using Gas Chromatography and Nile Red
594 Staining. Bio-Protocol 8:1–15.
595 36. Sartori A, Gatz R, Beck F, Rigort A, Baumeister W, Plitzko JM. 2007. Correlative
596 microscopy: Bridging the gap between fluorescence light microscopy and cryo-
597 electron tomography. J Struct Biol 160:135–145.
598 37. Schwartz CL, Sarbash VI, Ataullakhanov FI, Mcintosh JR, Nicastro D. 2007. Cryo-
599 fluorescence microscopy facilitates correlations between light and cryo-electron
600 microscopy and reduces the rate of photobleaching. J Microsc 227:98–109.
601 38. Dahlberg PD, Saurabh S, Sartor AM, Wang J, Mitchell PG, Chiu W, Shapiro L, Moerner
602 WE. 2020. Cryogenic single-molecule fluorescence annotations for electron
603 tomography reveal in situ organization of key proteins in Caulobacter. Proc Natl Acad

604 Sci U S A 117:13937–13944.
605 39. Tarazona NA, Hernández-Arriaga AM, Kniewel R, Prieto MA. 2020. Phasin interactome
606 reveals the interplay of PhaF with the polyhydroxyalkanoate transcriptional regulatory
607 protein PhaD in Pseudomonas putida. Environ Microbiol 22:3922–3936.
608 40. Pfeiffer D, Jendrossek D. 2011. Interaction between poly(3-hydroxybutyrate) granule-
609 associated proteins as revealed by two-hybrid analysis and identification of a new
610 phasin in Ralstonia eutropha H16. Microbiology 157:2795–2807.
611 41. Buckley RM, Stubbe JA. 2015. Chemistry with an artificial primer of
612 polyhydroxybutyrate synthase suggests a mechanism for chain termination.
613 Biochemistry 54:2117–2125.
614 42. Grant CR, Wan J, Komeili A. 2018. Organelle Formation in Bacteria and Archaea.
615 Annu Rev Cell Dev Biol 34:217–238.
616 43. Blakemore R. 1974. Magnetotactic Bacteria. Science (80-) 190:377–379.
617 44. Scheffel A, Gruska M, Faivre D, Linaroudis A, Plitzko JM, Schüler D. 2006. An acidic
618 protein aligns magnetosomes along a filamentous structure in magnetotactic bacteria.
619 Nature 440:110–114.
620 45. Uebe R, Keren-Khadmy N, Zeytuni N, Katzmann E, Navon Y, Davidov G, Bitton R,
621 Plitzko JM, Schüler D, Zarivach R. 2018. The dual role of MamB in magnetosome
622 membrane assembly and magnetite biomineralization. Mol Microbiol 107:542–557.
623 46. Raschdorf O, Forstner Y, Kolinko I, Uebe R, Plitzko JM, Schüler D. 2016. Genetic and
624 Ultrastructural Analysis Reveals the Key Players and Initial Steps of Bacterial
625 Magnetosome Membrane Biogenesis. PLoS Genet 12:1–23.
626 47. Hill NC, Tay JW, Altus S, Bortz DM, Cameron JC. 2020. Life cycle of a cyanobacterial
627 carboxysome. Sci Adv 6:1–8.
628 48. Ren Q, Roo G De, Ruth K, Witholt B, Zinn M. 2009. Simultaneous Accumulation and
629 Degradation of Polyhydroxyalkanoates : Futile Cycle or Clever Regulation ? 916–922.
630 49. Prieto A, Escapa IF, Martínez V, Dinjaski N, Herencias C, de la Peña F, Tarazona N,
631 Revelles O. 2016. A holistic view of polyhydroxyalkanoate metabolism in
632 Pseudomonas putida. Environ Microbiol 18:341–357.
633 50. Doi Y, Segawa A, Kawaguchi Y, Kunioka M. 1990. Cyclic nature of poly(3-
634 hydroxyalkanoate) metabolism in Alcaligenes eutrophus. FEMS Microbiol Lett 165–
635 169.
636 51. Taidi B, Mansfield DA, Anderson AJ. 1995. Turnover of poly(3-hydroxybutyrate) (PHB)
637 and its influence on the molecular mass of the polymer accumulated by Alcaligenes
638 eutrophus during batch culture. FEMS Microbiol Lett 129:201–205.

639 52. Buckley RM. 2013. The role of the phasin PhaP in promoting polyhydroxybutyrate (
640 PHB) granule formation in Caulobacter crescentus.
641 53. Jossek R, Steinbüchel A. 1998. In vitro synthesis of poly(3-hydroxybutyric acid) by
642 using an enzymatic coenzyme A recycling system. FEMS Microbiol Lett 168:319–324.
643 54. Juengert JR, Patterson C, Jendrossek D. 2018. Poly(3-Hydroxybutyrate) (PHB)
644 Polymerase PhaC1 and PHB Depolymerase PhaZa1 of Ralstonia eutropha Are
645 Phosphorylated In Vivo. Appl Environ Microbiol 84:e00604-18.
646 55. Bresan S, Jendrossek D. 2017. New Insights into PhaM-PhaC-Mediated Localization of
647 Polyhydroxybutyrate Granules in Ralstonia eutropha H16. Appl Environ Microbiol
648 83:1–14.
649 56. Pfeiffer D, Jendrossek D. 2014. PhaM Is the Physiological Activator of Poly(3-
650 Hydroxybutyrate) (PHB) Synthase (PhaC1) in Ralstonia eutropha. Appl Environ
651 Microbiol 80:555–563.
652 57. Pfeiffer D, Wahl A, Jendrossek D. 2011. Identification of a multifunctional protein,
653 PhaM, that determines number, surface to volume ratio, subcellular localization and
654 distribution to daughter cells of poly(3-hydroxybutyrate), PHB, granules in Ralstonia
655 eutropha H16. Mol Microbiol 82:936–951.
656 58. Maehara A, Taguchi S, Nishiyama T, Yamane T, Doi Y. 2002. A repressor protein,
657 PhaR, regulates polyhydroxyalkanoate (PHA) synthesis via its direct interaction with
658 PHA. J Bacteriol 184:3992–4002.
659 59. Yamada M, Takahashi S, Okahata Y, Doi Y, Numata K. 2013. Monitoring and kinetic
660 analysis of the molecular interactions by which a repressor protein, PhaR, binds to
661 target DNAs and poly[(R)-3-hydroxybutyrate]. AMB Express 3:3–9.
662 60. Thanbichler M, Iniesta AA, Shapiro L. 2007. A comprehensive set of plasmids for
663 vanillate - And xylose-inducible gene expression in Caulobacter crescentus. Nucleic
664 Acids Res 35.
665 61. Mastronarde DN. 2003. SerialEM: A program for automated tilt series acquisition on
666 Tecnai microscopes using prediction of specimen position. Microsc Microanal 9:1182–
667 1183.
668 62. Dahlberg PD, Sartor AM, Wang J, Saurabh S, Shapiro L, Moerner WE. 2018.
669 Identification of PAmKate as a Red Photoactivatable Fluorescent Protein for Cryogenic
670 Super-Resolution Imaging. J Am Chem Soc 140:12310–12313.
671 63. Dahlberg PD, Perez D, Hecksel CW, Chiu W, Moerner WE. 2022. Metallic support films
672 reduce optical heating in cryogenic correlative light and electron tomography. J Struct
673 Biol 214:107901.

674 64. Kremer JR, Mastronarde DN, McIntosh JR. 1996. Computer visualization of three-
675 dimensional image data using IMOD. J Struct Biol 116:71–76.
676
677

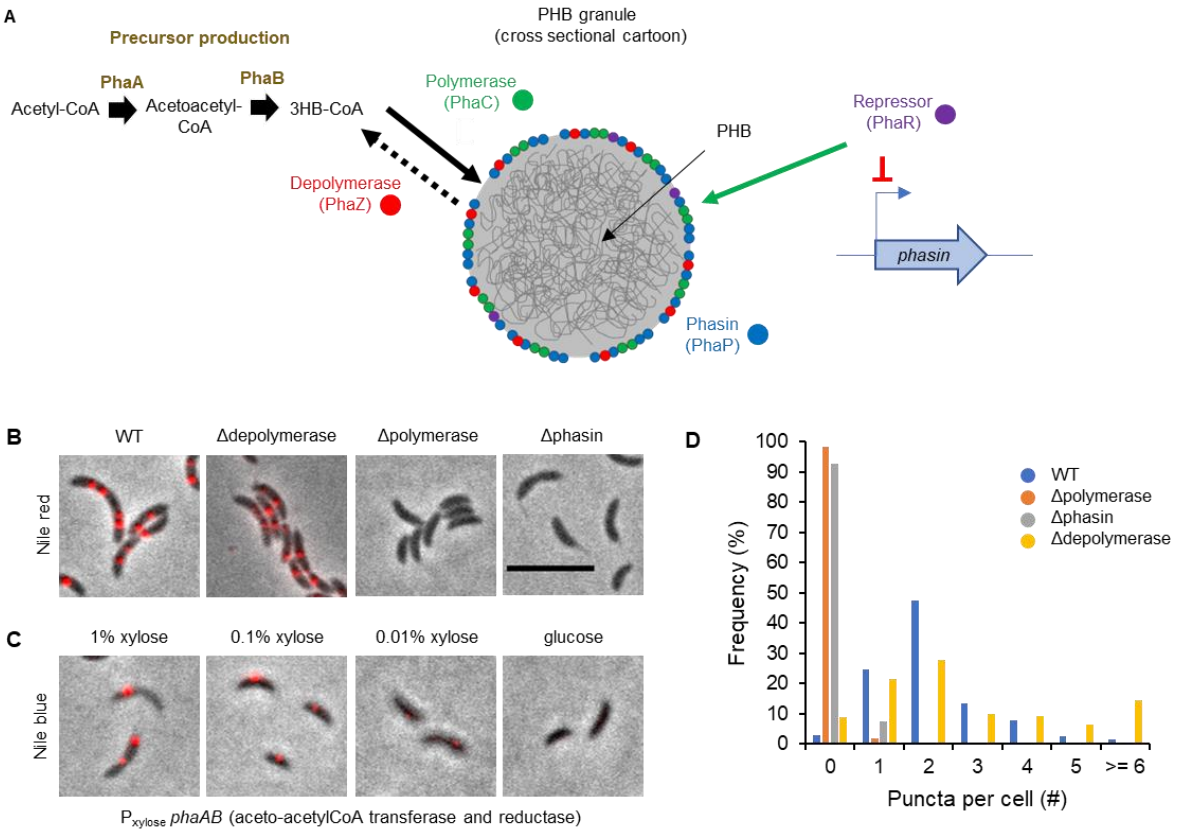

Figure 1. WT PHB granule formation requires both active polymerase and phasin

A) Schematic of PHB granule organization. A PHB granule consists mainly of water-insoluble PHB, with granule associated proteins on its surface (7). PHB is synthesized by the polymerase PhaC using the 3HB-CoA precursor. This precursor is generated from acetyl-CoA by PhaA and PhaB (23). PHB is consumed by the depolymerase PhaZ, possibly with uncharged CoA as an acceptor for released monomers. Both PhaC and PhaZ are associated with the granule, while PhaA and PhaB are not (8). Another abundant granule associated protein is phasin (PhaP). Its expression is regulated by the transcriptional repressor PhaR, which itself is sequestered to the granule upon PHB synthesis (13, 14). **B)** Deletion of either polymerase PhaC or phasin PhaP results in a loss of nile-red stained granules. Overlay images of phase contrast and Nile-Red fluorescence. Cells are stained in PBS with 1 μM nile red for 20 minutes. Strains used are WT, ΔphaZ (LS5811), ΔphaC (LS5813) and ΔphaP (LS5812). Scale bar is 5 μm. **C)** Reducing precursor availability results in a reduction in nile blue signal and loss of stained granules. Overlay images of phase contrast and nile blue fluorescence. Cells are stained M2G with 10 μM nile blue for 20 minutes. The strain contains a xylose inducible promoter at the start of the CCNA_00544-00545 (phaA-phaB) operon (LS5814). Strain LS5814 was grown for 5 hours in the presence of xylose % as indicated. **D)** Quantification of (B), at least 600 cells were analyzed per strain.

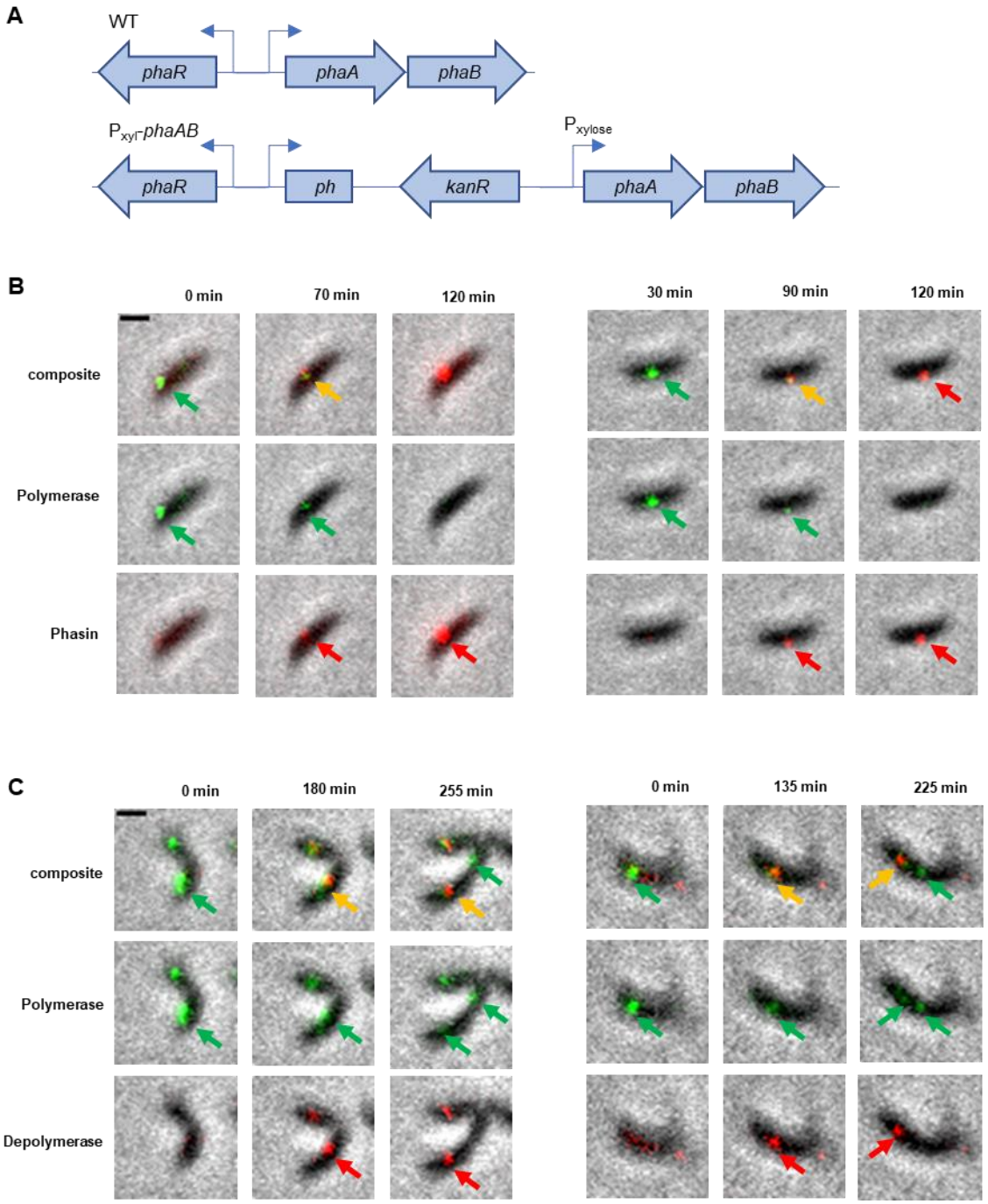

Figure 2. Polymerase condensation precedes phasin and depolymerase condensation

A) Representation of the xylose inducible *phaAB* operon (strain LS5814). The genomic region containing *phaR* (CCNA_00543), *phaA* (CCNA_00544) and *phaB* (CCNA_00545) is shown for the WT (top). The xylose inducible promoter was introduced by single crossover integration targeting the 5' 800bp of *phaA*, leading to a truncated duplication controlled by the WT transcription start site, while the full *phaAB* operon is under control of the xylose promoter. **B)** Timelapse of granule formation. Granule formation was induced by the addition of 1% xylose just prior to timelapse microscopy. Granule formation was visualized

712 by fluorescence imaging of polymerase-GFP and phasin-mCherry (strain LS5871).
713 Condensation of Polymerase is indicated by a green arrow, condensation of phasin by a red
714 arrow, and co-localization by a yellow arrow. Scale bar is 1 μm. **C)** Timelapse of granule
715 formation following glucose introduction to glucose-starved cells. Granule formation was
716 visualized by fluorescence imaging of polymerase-GFP and depolymerase-mCherry (strain
717 LS5821). Condensation of polymerase is indicated by a green arrow, condensation of
718 depolymerase by a red arrow, and co-localization by a yellow arrow. Scale bar is 1 μm.
719

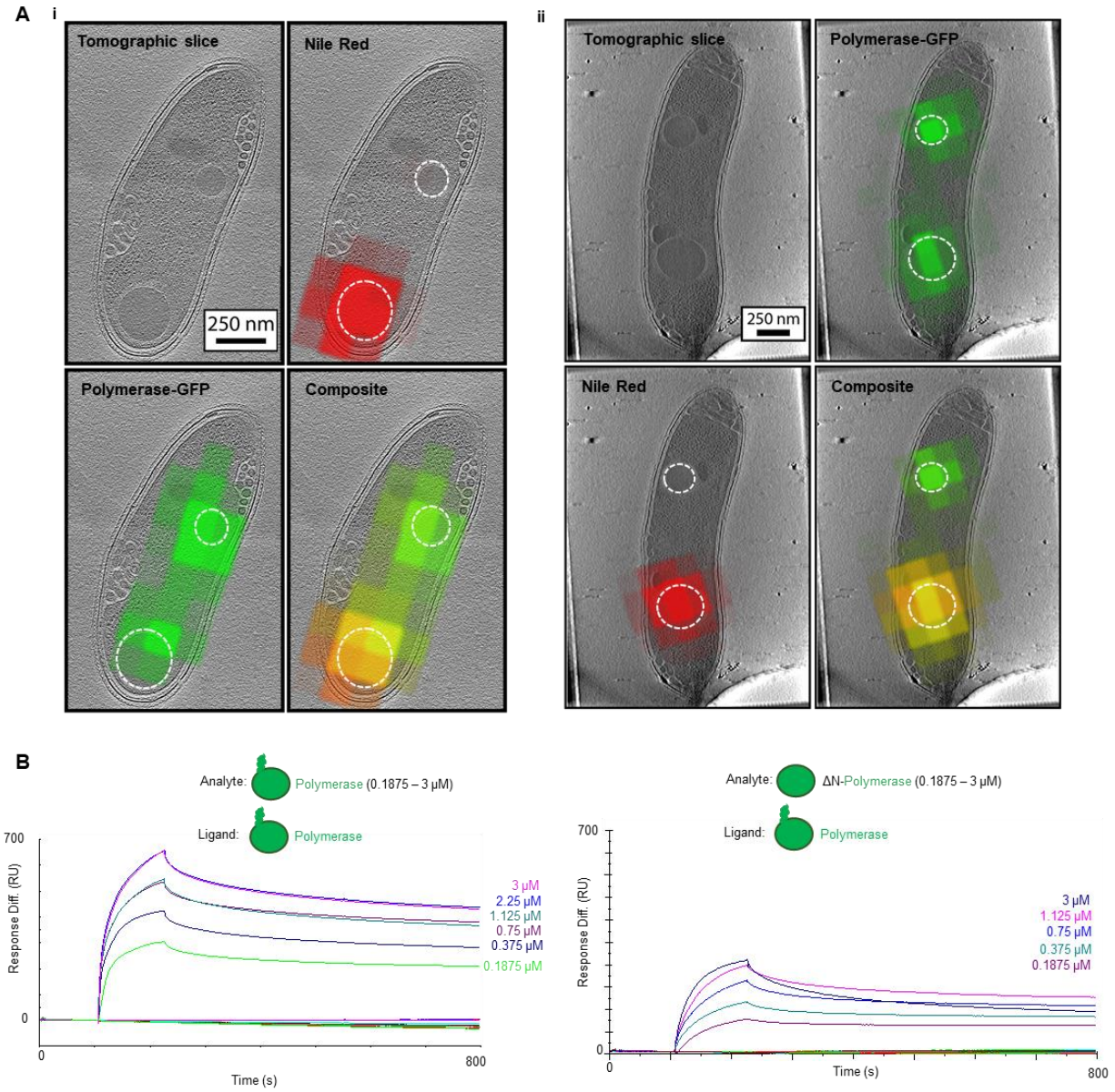

Figure 3. Granule maturation as shown by cryo-CLEM and polymerase self-interaction shown by SPR

A) Examples of cells expressing polymerase-GFP (strain LS5810) and PHB granule stained with Nile Red. i) A tomographic slice from a 3D reconstruction (top left) shows 2 granules in this cell. The polymerase-GFP signal (green) co-localizes with both these granules (bottom left). However, only the larger granule stains for Nile-Red (top right). A composite image shows the co-localization of polymerase-GFP and Nile-Red in yellow in the larger granule (bottom right). PHB granules are outlined in the overlay images by a dotted circle. ii) Another example cell. **B)** Purified polymerase was tested for self-interaction in vitro using surface plasmon resonance. Polymerase was immobilized on the surface using amine crosslinking as ligand, and either full-length polymerase (left graph) or the N-terminal mutant polymerase, which lacks the first 85 amino acids on the N-terminus (right graph), were flown over as analyte at increasing concentrations as indicated.

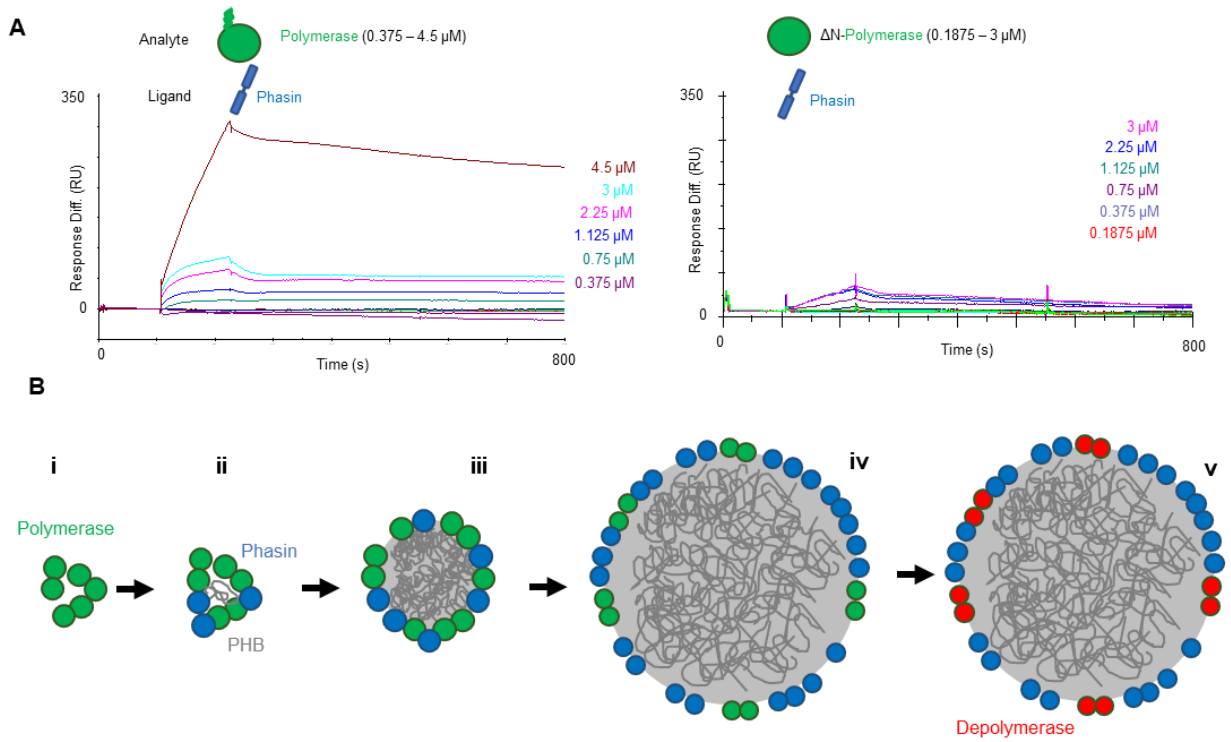

Figure 4. Phasin and Polymerase interact directly through polymerase N-terminus.

A) Polymerase binds immobilized phasin, but polymeraseΔN does not. Surface plasmon resonance response curves of either polymerase (left graph) or polymeraseΔN (right graph) flown over surface immobilized phasin at increasing concentrations as indicated. **B)** Proposed model for PHB granule formation. i) Polymerase self-interaction (Fig. 3B) promotes condensation that precedes the condensation of phasin (Fig. 2B). ii) Polymerase recruits phasin through direct interaction (Fig. 4A), forming a nascent granule possibly assisted by the early initiation of PHB polymer formation. iii) Ongoing PHB synthesis expands the granule size. iv) As the PHB granule grows until its mature size, more phasin is recruited. v) Once the granule reaches its mature size, the PHB polymerase dissociates from the granule, coincident with the recruitment of the PHB depolymerase (Fig 2C).

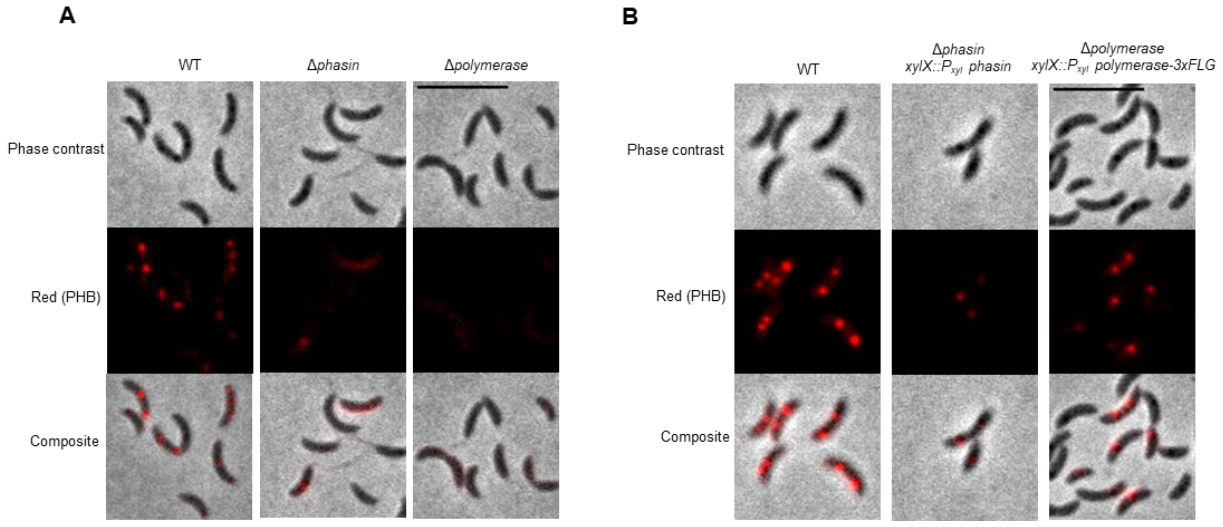

Figure S1. WT and mutants stained by nile blue dye.
A) Deletion of either polymerase PhaC or phasin PhaP results in a loss of nile-blue stained granules. Strains used are WT, LS5812 and LS5813. Cells are incubated for 20 minutes with Nile Blue prior to imaging. Nile Blue stained PHB granules can be visualized in the red channel (554nm/609nm excitation/emission). Scale bar is 5 μm. **B)** Complementation of polymerase and phasin deletion mutants. A copy of either *phasin* or *polymerase-3xFLAG* was expressed from the xylose locus (*xylX*) using a xylose inducible promoter. Cells were grown in presence of 0.1% xylose in M2G media and PHB granules were visualized using Nile-Blue staining. Strains used are WT, LS5826 and LS5872. Scale bar is 5 μm.

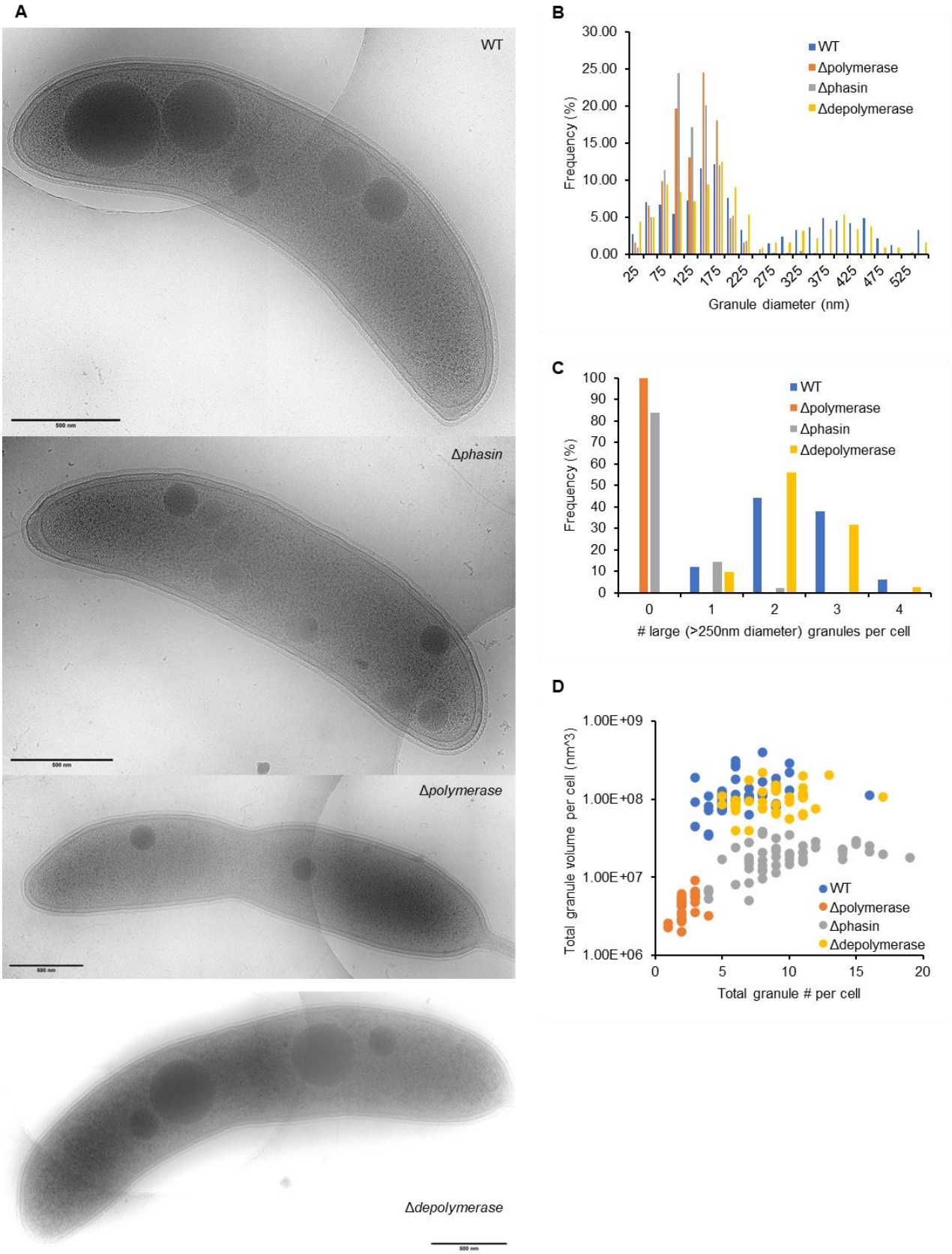
A
WT
Δphasin
Δpolymerase
Δdepolymerase
B
Frequency (%)
Granule diameter (nm)
WT
Δpolymerase
Δphasin
Δdepolymerase
C
Frequency (%)
large (>250nm diameter) granules per cell
WT
Δpolymerase
Δphasin
Δdepolymerase
D
Total granule volume per cell (nm^3)
Total granule # per cell
WT
Δpolymerase
Δphasin
Δdepolymerase

761
762

763 **Figure S2. Granule quantification by cryo electron microscopy.**
764 **A)** Cryo electron micrographs of WT (top), Δ*phasin* (middle-top, LS5812), Δ*polymerase*
765 (middle-bottom, LS5813) and Δ*depolymerase* (bottom, LS5811) cells. Scale bar is 500 nm.
766 **B)** Frequency of granule diameters measured from 25-50 cells per sample. All granules are
767 measured, so this includes both PHB and poly-P granules. Only poly-P granules were
768 observed in the Δ*polymerase* cell. **C)** Frequency of granule diameters for granules with a
769 diameter >250nm. **D)** Total cumulative granule volume per cell. Granule volumes were
770 calculated based on granule diameters, and all granule volumes were summed per cell.
771 Although Δ*phasin* cells have more granules per cell than WT (9.8 vs 6.6 granules per cell),
772 the total granule volume per cell is 6.6x lower than WT.
773
774 In EM images, both PHB and poly-phosphate granules can be found in WT cells. Although
775 poly-phosphate granules have been reported to be more electron dense than PHB granules
776 (6), we were unable to quantify such a difference in our images. Since cells lacking the PHB
777 polymerase will only contain poly-phosphate granules, we used this as the expected average
778 number of poly-phosphate granules per cell. In Δpolymerase cells there were on average 2.3
779 granules per cell at an average 143nm diameter. We observed no granules with a diameter
780 over 250nm in Δpolymerase cells, which we assume will be the maximum diameter for poly-
781 phosphate granules. WT cells contain both PHB and poly-P granules, on average 6.6 granules
782 per cell. On average 2.4 granules per cell have a diameter that exceeds 250nm, comparable
783 to the average of 2.1 Nile Red stained granules per cell (Fig. 1D), which should only stain PHB
784 granules. The remaining granules (on average 4.2 per cell) that do not exceed 250nm
785 therefore are likely a mix of poly-phosphate granules and smaller PHB granules. For the phasin
786 mutant we observe on average 9.8 granules per cell, of which only 0.2 granules per cell
787 exceed 250nm diameter. This subset (16.3%) of the cells reflects the 7.3% cells containing
788 Nile red stained granules (Fig. 1D).
789

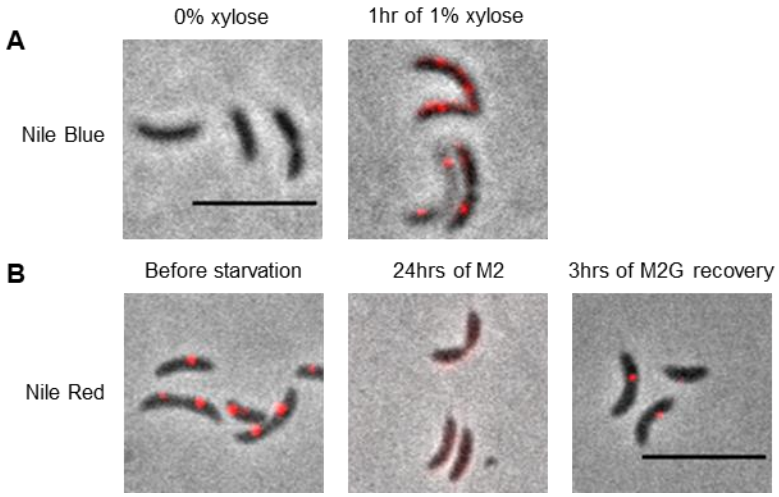

Figure S3. Controlled granule formation in *Caulobacter*
A) Cells with PhaAB expression under xylose control (LS5814) do not show any Nile Blue puncta in the absence of xylose (left). Addition of 1% xylose results in clear Nile Blue puncta after only 1 hour of growth (right). **B)** WT cells grown into stationary phase in M2Glucose show clear Nile Red puncta (left). Replacing the media with M2 and starving the cells for 24 hours results in a loss of Nile Red puncta (middle). Replacing the media again with M2Glucose recovers the Nile Red puncta after 3 hours (right). Scale bars are 5μm.

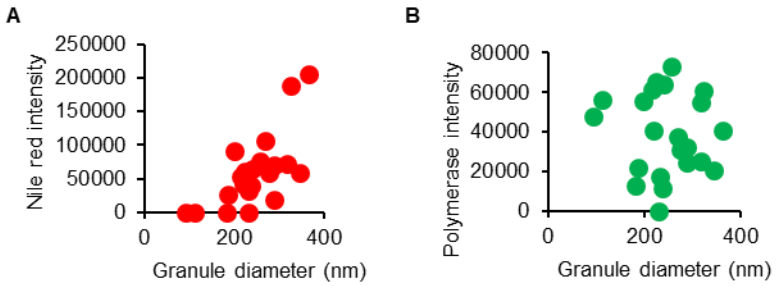

Figure S4. Nile Red intensity correlates to PHB granule size.
Quantification of **A)** Nile Red and **B)** Polymerase-GFP signal of cryo-CLEM images. Fluorescent intensities were measured for 22 granules and compared to the diameter of these granules. Only granules that had Nile Red and/or GFP signal were analyzed. A positive correlation is observed between granule diameter and Nile Red intensity (A), while no correlation is seen between granule diameter and polymerase-GFP signal.

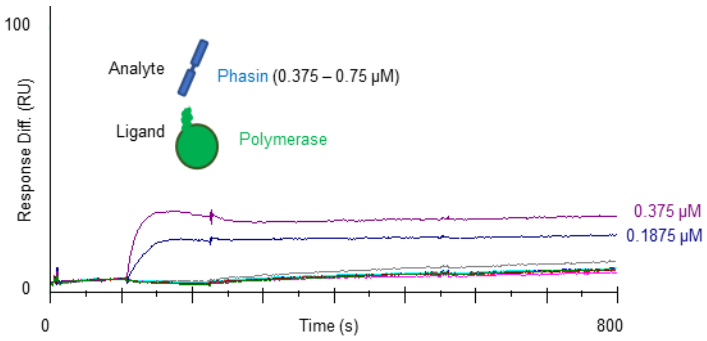

Figure S5. Phasin binds immobilized Polymerase in SPR
Surface plasmon resonance response curves of increasing concentrations of phasin flown over surface immobilized polymerase at increasing concentrations as indicated.

812 **Table S1. Bacterial strains**

813 A. List of *Caulobacter* strains used in this study. Plasmids integrate either by single- (:) or
814 double- (::) crossover.

Name	Genotype	Source
LS101 (WT)	NA1000/CB15N	Lab strain
LS5811	CCNA_00250::tetR	LS101::pEK012
LS5813	CCNA_01444::rifR	LS101::pEK014
LS5812	CCNA_02242::catR	LS101::pEK013
LS5814	CCNA_00544:Pxyl-CCNA_00544 kanR	LS101:pEK022
LS5810	CCNA_01444:CCNA_01444-GFP gentR	LS101:pEK005
LS5809	CCNA_02242::CCNA_02242-mCherry	LS101::pEK003
LS5816	CCNA_02242::CCNA_02242-mCherry, CCNA_01444:CCNA_01444-GFP gentR	LS5809:pEK003
LS5871	CCNA_02242::CCNA_02242-mCherry, CCNA_01444:CCNA_01444-GFP gentR, CCNA_00544:Pxyl-CCNA_00544 kanR	LS5816::pEK022
LS5819	CCNA_00250::CCNA_00250-mCherry	LS101::pEK044
LS5821	CCNA_00250::CCNA_00250-mCherry, CCNA_01444:CCNA_01444-GFP gentR	LS5819:pEK003
LS5872	CCNA_02242::catR, xylX:Pxyl CCNA_02242 kanR	LS5812:pEK055
LS5826	CCNA_01444::rifR, xylX:P_{xyl}-CCNA_01444-3xFLAG kanR	LS5813::pEK052

815

816 B. List of *E. coli* strains used in this study.

Name	**Source**
Ultracompetent DH5α	New England Biolabs
BL21(DE3)	Novagen

817

818

819 **Table S2. Plasmids and primers**

820 A. List of plasmids used in this study.

Identifier	Plasmid	Source
pET28a	Plasmid for IPTG inducible His-tag protein purification	Novagen (lab strain)
pNPTS138	*Caulobacter* sucrose counterselection integration plasmid	(60)
pCHYC-1	Plasmid for C-terminal tagging with mCherry, specR	(60)
pGFPC-4	Plasmid for C-terminal tagging with GFP, gentR	(60)
pMCS-3	Plasmid containing rifampicin resistance cassette	(60)
pMCS-5	Plasmid containing tetracycline resistance cassette	(60)
pMCS-6	Plasmid containing chloramphenicol resistance cassette	(60)
pXMCS-2	Plasmid for xylose induction at native locus	(60)
pXCHYC-2	Plasmid for xylose induction at *xylX* locus	(60)
pTC88	Plasmid containing *pleC*-3xFLAG	Chong *et al.*, 2023 (update reference)
pTC127	Plasmid containing *pleC*-3xFLAG integrating at *xylX*	Chong *et al.*, 2023 (update reference)
pEK001	pET28a 6xHis-CCNA_01444	This study
pEK003	pNPTS138 CCNA_02242-mCherry	This study
pEK005	pGFPC-4 CCNA_01444-GFP	This study
pEK011	pET28a 6xHis-CCNA_02242	This study
pEK035	pET28a 6xHis-CCNA_01444 (256-2016bp)	This study
pEK039	pNPTS138 ΔCCNA_00543	This study
pEK044	pNPTS138 CCNA_00250-mCherry	This study
pEK052	pNPTS138 CCNA_01444-3xFLAG	This study
pEK055	pXCHYC-2 CCNA_02242	This study

821

822 B. List of primers used for strain construction.

Identifier	Sequence
EKP001	cgcgcggcagccatatggctagcATGGCCACGGCGAAGGCCGCCC
EKP002	cgacggagctgaattcggatccTCAGGGTTGTGACTTTACCAGCACAAA
EKP003	cgcgcggcagccatatggctagcATGCTCTACGCCCTGACACGAGG
EKP004	cgacggagctgaattcggatccTCAGACTTCCTCGCCGAAGTTCG
EKP005	tgaagccggctggcgccaagcttACCGGCAAGACACGTCAGGGCC
EKP006	taaggtaccGCGGGCGGCCTGGAACTTTTCG
EKP007	gccgcccgcGGTACCTTAAGATCTCGAGCTCCGGAGAATTCG
EKP008	gagcaggccGGATCCCCCGGGCTGCAGCTAG
EKP009	gggggatccGGCCTGCTCCAGGCGCGCTCAC
EKP010	gacgcgtcacggccgaagctagcGATGCCGTAATCGTGCGCGCAGGC
EKP015	gttttggggagacgaccaatgagcgagattgtcatcgtttccgccgcc
EKP016	gagctcaccacgtggtaccgccgcgcttggcggcttcctcg
EKP071	ttggggagacgaccatatgATGGCCGCGGCCGAAAACCTG
EKP074	tccccccgggctgcagctagcTTAGCGGGCGGCCT
EKP083	cgaattctccggagctGGTTGTGACTTTACCAGCACAAATG
EKP084	ttggggagacgaccatatgGCCACGGCGAAGG
EKP085	ttggggagacgaccatatgGTCGAGACCCTCTCGG
EKP086	CGTAGGCTACGCCATCGGCGGCACCCTGCTCTCG
EKP087	GCCGCCGATGgCGTAGCCTACGGTGTTGACGCG
MP001F	tcactagtggggcccgtgcaattgaagccggctggcgccaagcttGGCCGCTTCGACTTCCAC
MP001R	gctcgagatcttaaggtaccGACTTCCTCGCCGAAGTTCG
MP002F	CGAACTTCGGCGAGGAAGTCggtaccttaagatctcgagctccg
MP002R	GCCGCAAGAGCGACCCTACGggatcccccgggct
MP003F	agctgcagcccgggggatccCGTAGGGTCGCTCTTGCG
MP003R	gacgcatgcctgtacatccggagacgcgtcacggccgaagctagcCCTGAGCTTGTCGAAGGACG

823

824